Strain Sensor with Both a Wide Sensing Range and High Sensitivity Based on Braided Graphene Belts

Yuxiang Li, Tengyu He, Liangjing Shi, Ranran Wang,* and Jing Sun*

Read Online

ACCESS | Metrics & More | Article Recommendations | Supporting Information

ABSTRACT: Recent years have witnessed significant development of flexible strain sensors in a variety of fields. Nevertheless, the challenge of integrating a broad sensing range (>50%) with high sensitivity [gauge factor (GF) value > 100 over the entire sensing strain] in one single flexible strain sensor still exists. Herein, we prepared a flexible strain sensor based on braided graphene belts (BGBs) and dragon skin. Such a BGB strain sensor exhibits an integration of a wide sensing range (up to 55.55%) and high sensitivity (GF value > 175.16 through the entire working range). Besides, this BGB strain sensor also demonstrates a minute monitoring limit (0.01%), low hysteresis and overshoot behaviors, and reliable cycling repeatability (>6000 cycles). The SEM microscopy observations reveal that the skew angle and intersection regions of graphene belts are mainly responsible for the desirable sensing performance. Finally, the successful detection of full-range human motions, from subtle actions to vigorously joint-related movements, reflects great potential of the BGB strain sensor in the application of wearable instruments.

KEYWORDS: flexible strain sensor, braided graphene belts, sensing range, sensitivity, skew angle, intersection regions
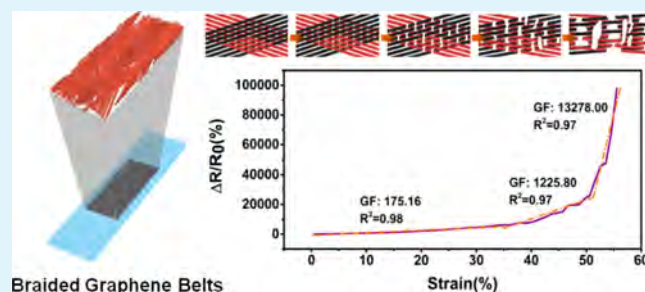
1. INTRODUCTION

Flexible strain sensors, compared with conventional strain sensors composed of metals[1] or semiconductor materials,[2] show superior application potentials in a diverse array of fields covering personal healthcare,[3] sports performance monitoring,[4] human−machine interfaces,[5] virtual reality,[6] and so forth.[7−9] This can be attributed to their own merits like light weight, flexibility, biocompatibility, and so forth.[10−12] The parameters,[13] including sensing range, sensitivity or gauge factor (GF), response time, detection limit, hysteresis, overshoot, durability, and so on, are often employed to evaluate the sensing properties of the flexible strain sensors. Among these indicators, sensing range and sensitivity are the most significant, as the former is the key in determination of the application range of the flexible strain sensors, and the latter reflects the flexible strain sensors' response capabilities to the variation of the tensile strain. Nowadays, the emerging flexible strain sensors should possess both broad sensing range (>50%) and high sensitivity (GF value > 100 among the whole working range),[14] so that they can be successfully applied to full-range human activities' monitoring, from subtle actions (e.g., voice rehabilitation, expiration, heartbeat, pulse, and so on) to vigorously joints-related behaviors (e.g., finger bending, running, jumping, etc.).[15] Nevertheless, it seems a challenge to accomplish the coupling of a wide sensing range and high sensitivity in one single flexible strain sensor. Because, for one thing, in order to achieve a broad sensing range, flexible strain

sensors need to keep conductive pathways from destruction upon considerable stretch, for another, to realize high sensitivity, the sensing film needs to experience considerable structure deformation under tensile strain.

To tackle this issue, one important strategy is to design the microstructure of the sensing film. A variety of microstructures have been created to enhance the sensitivity or the sensing range of strain sensors.[6,11,16−19] For instance, Kang et al.[18] prepared a Pt-based flexible strain sensor inspired from the slit organ of the spider. This strain sensor exhibited an impressively high sensitivity (GF value > 2000) because of the elongation of cracks under stretching. Nevertheless, the sensing range was only 2%. Wang et al.[19] fabricated a graphene-based flexible strain sensor by copying the microstructure of woven copper fabrics. Despite ultrahigh sensitivity (up to 10^3) under a small tensile strain from 2 to 6%, also because of the rapid initiation and fast propagation of cracks under tensile strain, this strain sensor showed a limited sensing range (10−12%). Wrinkles or buckles are generally constructed to improve the sensing range of sensing materials,
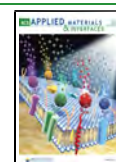
which however will sacrifice the sensitivity.[20−22] Liu et al.[21] proposed a flexible strain sensor with an Au film possessing the wrinkle structure. The wrinkle structure endowed this Au-based strain sensor with a sensing range of 130% strain, but a GF value of around 0.74. He et al.[22] reported a flexible strain sensor based on multilayered graphene woven fabrics designed from the gradient of buckle wavelength through graphene layers. This strain sensor demonstrated a high working range (242.74%), but the sensitivity was low (GF value > 1 for the whole sensing range). In addition, the fabrication of the strain sensor needed the process of repeated transferring, prestretching, and releasing of graphene woven fabrics many times, which was very intricate and time-consuming. Therefore, novel microstructures and the corresponding fabrication methods should be further explored for the realization of both a broad sensing range and high sensitivity in one single flexible strain sensor.

A braided Cu belt is composed of interlaced conductive bundles, and there are a bunch of copper wires parallelly arranged in a bundle. When the sensing film is patterned from braided Cu belts, a number of conductive circuits will form in the sensing layer. Two advantages can be expected from this pattern. For one thing, the braided sensing belts composed of fibers interweaving in a skew way can rotate when they are subjected to large tensile strain, which would dissipate strain energy and keep the intactness of the conducting paths, thus ensuring a broad sensing range of the flexible strain sensor. For another, the intersection regions of the sensing belts with different orientations can be considered as the districts of stress concentration, where cracks can rapidly initiate when the flexible strain sensor is under stretching, triggering the drastic augmentation of resistance, and therefore guaranteeing high sensitivity over the whole sensing range.

Inspired by the merits of braided Cu belts, herein, we reported a facile strategy of fabricating a braided graphene belt (BGB)-based strain sensor with the sensing layer replicated from braided Cu belts. As a demonstration, such a BGB strain sensor exhibits not only a broad sensing range (up to 55.55%), but also high sensitivity over the whole sensing strain (GF value > 175.16). Additionally, the BGB strain sensor also possesses an ultralow detection limit (0.01%), low hysteresis and overshoot behaviors, and reliable cycling repeatability (>6000 cycles). Such an incorporation of excellent sensing performance indicators provides the BGB strain sensor with great capability of full-range human motions' monitoring, from subtle stimuli (e.g., voice recognition, expiration, heartbeat, and pulse) to vigorous joint behaviors (e.g., finger-bending movements and knee-related activities such as jogging, jumping, and squatting).

2. EXPERIMENTAL SECTION

2.1. Preparation of the BGBs. The braided Cu belts (∼140 μm in diameter per wire, commercially available) were cut into pieces of 6 × 1 cm^2, followed by ultrasonication treatment with acetone (acetone, >99.5%, AR, Shanghai Lingfeng Chemical Reagent Co., Ltd.) and subsequently diluted HCl (HCl/deionized water = 10:30 mL) (hydrochloric acid, 36−38%, GR, Greagent, Shanghai Titan Scientific Co., Ltd.) for the removal of surface contamination and the oxide layer. Afterward, the as-treated pieces were put into a quartz tube and then heated to 1000 °C in 1 h with a flowing gas mixture (H$_2$/Ar = 100:1000 mL/min), then annealed at 1000 °C for 30 min. Subsequently, the flowing gas mixture was altered (H$_2$/Ar = 45:400 mL/min) and remained for 5 min, and CH$_4$ (65 mL/min) was then introduced to start the growth of graphene (growth temperature at

1000 °C). After 30 min, the quartz tube was quickly cooled down to room temperature. The braided Cu-graphene belts were cut into shapes of L × 1 cm^2 (L is the length of the belts depending on the need of different strain sensors.) and then adhered to the thermal-released tape (viscosity failure temperature of 120 °C, commercially available). The above sample was put onto the etchant solution composed of 0.5 mol/L HCl and 0.5 mol/L FeCl$_3$ (Iron (III) Chloride, 99%, RG, Adamas-beta, Shanghai Titan Scientific Co. Ltd.) and copper wires were etched away. The remained BGBs were rinsed with deionized water.

2.2. Preparation of the BGB Strain Sensor. The dragon skin (10 Medium, Smooth-On inc.) was poured into the mold (with the size of 6 cm × 1.5 cm × 1 mm), and then put into the vacuum oven to remove the bubbles and precured at 80 °C for 0, 1.5, and 3 min, respectively. The BGBs with the thermal-released tape were stuck on the as-precured dragon skin, followed by being cured at 80 °C for 2 h and subsequently cooled down to room temperature. Afterward, the BGBs with the thermal-released tape were heated to 120 °C for 10 min to remove the thermal-released tape. The BGBs with dragon skin composite films were peeled from the mold. Finally, two Cu conductive wires were separately adhered onto the two sides of the BGBs with Ag paste, and the BGB strain sensor was obtained.

2.3. Characterization. The morphologies of the braided Cu belts and braided Cu−graphene composite belts were characterized by a field emission scanning electron microscope (TESCAN MIRA3, Czech Republic). The morphologies of the BGB strain sensor were characterized utilizing FE-SEM (Hitachi SU8220, Japan). The Raman characterization was carried out using DXR Raman Microscopy (Thermal Scientific Corporation, USA, with an excitation length of 532 nm). The electromechanical properties of the BGB strain sensor were tested using the system composed of a highly precise motorization linear stage (a displacement resolution of 2.5 μm) for the application of tension strain, an electrochemical station (PARSTAT 2273 Princeton Applied Research) to provide a constant voltage (0.1 V), and a software system to record real-time electric signals under stretching loadings. The software Image-Pro-Plus 6 was applied to the quantitative analysis of the scanning electron microscopy (SEM) photographs. The finite element analysis was carried out using the software COMSOL Multiphysics 5.3a to analyze the location change of the braided sensing belts before and after stretching, and the distribution of stress and strain in the braided sensing belts during tensile loading. To simplify the analysis, only two sensing belts were selected to do the modeling.

3. RESULTS AND DISCUSSION

3.1. Fabrication and Morphology Characterization of the BGB Strain Sensor. Figure 1a illustrates the fabrication procedure of the BGB strain sensor. In general, braided Cu belts were used as the template to obtain graphene belts through chemical vapor deposition. As shown in Figure S1a−d, the graphene covered the surface of Cu. Subsequently, the braided Cu−graphene belts were adhered to the thermal-released tape, and then Cu belts were etched away, during which the BGBs formed on the thermal-released tape. The BGBs on thermal-released tape were transferred to the precured dragon skin, following by postpolymerization at 80 °C for 2 h. Later, the thermal-released tape was peeled off through heating, and the BGB/dragon skin composite film was obtained. Finally, BGBs were connected with conductive wires at two ends using silver paste to obtain the BGB strain sensor. As shown in Figures 1b and S2, the BGB strain sensor is flexible and even bendable. The Raman spectrum of the BGB strain sensor in Figure S3 clearly shows the typical bands of graphene, namely, D-band (∼1352 cm^{-1}), G-band (∼1585 cm^{-1}) and G′-band (∼2694 cm^{-1}), revealing the sensing layer consisting of graphene with structure defects.[23] In addition, the value of $I_{G'}/I_G$ is approximately 0.147, and the full width at
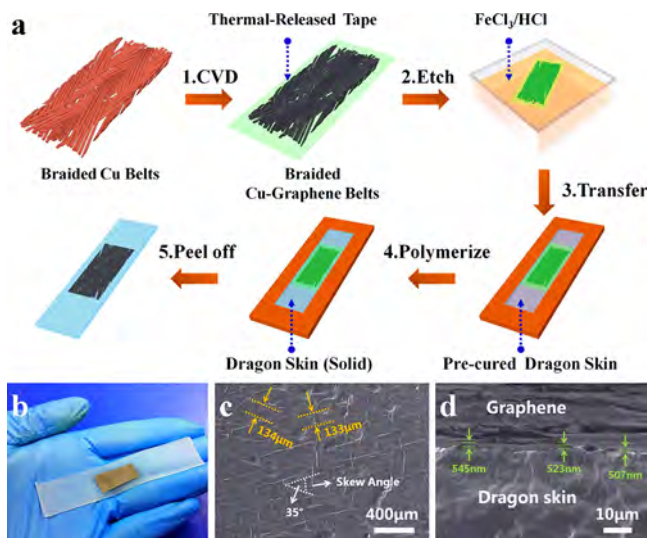
Figure 1. Schematic illustration of the fabrication and the characterization of the BGB strain sensor. (a) Preparation process of the BGB strain sensor (for simplicity, only one layer of braided Cu belts is shown in the schematic graph). (b) Optical photograph of the BGB sensing film. (c) Top-view SEM image of the BGB strain sensor (the width of single graphene belt is marked to be around 133−134 μm via orange dotted lines and arrows, whereas the white dotted parts represent the skew angle between belts with different orientations.). (d) Cross-sectional SEM image of the BGB strain sensor.

half-maximum of the G′-band is around 85.816 cm^{-1}, standing for the multilayered configuration of graphene.[24]

Figure 1c presents an SEM image of the top-viewed BGB strain sensor, in which the graphene film replicates the pattern of braided Cu belts. After etching away Cu wires, the hollow belts collapsed into flattened ones and braided with each other. The skew angle, defined as the acute angle between the skewed interweaved belts with different orientations, as shown in Figure 1c, is around 35°. Besides, the width of each belt is about 133−134 μm, very close to that of a single Cu belt (~140 μm, demonstrated in Figure S1a). The cross-sectional SEM image shown in Figure 1d reveals a clearly identified interface between the BGBs and the dragon skin, despite the patterned sensing layer being strongly adhered to the flexible substrate. Furthermore, the conductive film possesses a layered structure, and the average film thickness is approximately 525 nm, demonstrating the multilayered structure of graphene, which is consistent with the results of the Raman spectrum as discussed above.

3.2. Tensile Strain Sensing Performances of the BGB Strain Sensor.

To investigate the sensing properties of the BGB sensor during the tensile strain, a constant voltage (0.1 V) was applied at two ends of the sensing film and real-time current (I) upon different tensile strains (ε) was recorded. The parameter, relative resistance variation $\Delta R/R_0$ ($\Delta R = R - R_0$, R_0 refers to the resistance of the sensing layer before experiencing a stretch, whereas R represents the resistance of the sensing layer under the tensile loading state.), was determined by transforming the as-recorded current in accordance with Ohm's Law. Here, the sensing range is defined as the maximum strain when the sensing film loses conductivity, and the GF is defined as the linear slope of the $\Delta R/R_0 - \varepsilon$ curve.

Figure 2a illustrates the relative resistance variation curves of the BGB strain sensors with different precured times during tensile loading. It should be noted that all relative resistance variation curves of the three BGB strain sensors ascend with the increase of the strain. With the increase of the precured
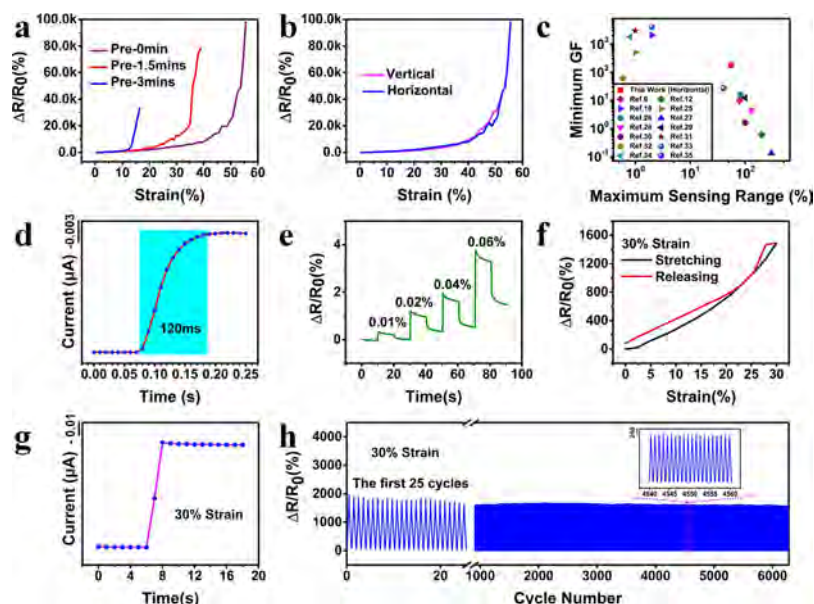

Figure 2. Tensile strain sensing behaviors of the BGB strain sensor. (a) Relative resistance variation versus tensile strain curves of the BGB strain sensors with various precured times (0, 1.5, and 3 min). (b) Relative resistance variation vs tensile strain curves of the BGB strain sensors with sensing films vertically and horizontally adhered on to the flexible substrate. (c) Summary and comparison of the sensing range and minimum GF from the reported literature and results in this work. (d) Current change of the BGB strain sensor under a sudden tension strain loading of 0.2%. (e) Relative resistance variation of the BGB strain sensor upon step tensile strains from 0.01 to 0.06%. (f) Relative resistance variation of the BGB strain sensor under the first stretching−releasing cycle at the strain of 30%. (g) Current change of the BGB strain sensor upon a quasitransient step strain loading of 30%. (h) Relative resistance variation of the BGB strain sensor under more than 6000 stretching−releasing cycles at the strain of 30%.

time, $\Delta R/R_0$ augments more quickly, wheras the sensing range descends. The sensing range of the BGB strain sensor with a precured time of 3 min is approximately 16.42%, and the GF is 103.46 in the strain range from 0 to 7.60%, 376.36 from 8.58 to 12.50%, and 8293.47 from 13.48 to 16.42%. With regard to the BGB strain sensor with the precured time of 1.5 min, the sensing range is 38.96%, and the value of GF changes from 169.01 within 21.07%, 1138.70 in the strain range of 22.07–34.98%, to 13,986.70 under a tensile strain of 35.98–38.96%. Despite high sensitivity under the whole strain sensing range for these two BGB strain sensors, they are still not desired for a number of flexible devices requiring a wider sensing range. In contrast, the BGB strain sensor with the precured time of 0 min possesses not only a broad sensing range of 55.55%, but also a large sensitivity of 175.16 within the tensile strain of 34.91%, 1225.80 within the strain of 35.89–49.65%, 13,278 from the tensile strain of 50.64 to 55.55%. As illustrated in Figure S4a–c, the longer the precured time, the more seriously the morphology of the BGBs breaks, and thus the narrower the sensing range obtained. In addition to the precured time, the effect of the arrangement of the graphene belts on the electromechanical properties of the BGB strain sensor was also investigated. The optical images of the graphene layer horizontally and vertically arranged on the substrate are shown in Figure S5a,b, respectively. As shown in Figure 2b, compared with the strain sensor with the graphene film horizontally arranged on the dragon skin substrate, the BGB strain sensor with the graphene film vertically arranged on the dragon skin substrate exhibits a strain sensing range of 54.33%, and the GF initiates from 116.69 within the strain of 30.53%, 933.42 for the strain of 31.52–45.40%, to 4447.88 under the strain from 46.39 to 54.33%. Such an incorporation of a broad sensing range and high sensitivity under the entire sensing strain makes the BGB strain sensor stand out against previous reports (Figure 2c and Table S1).[6,12,18,25–35] Based on the above results, the strain sensor with 0 min precured time and the graphene film horizontally arranged on the substrate was selected to be further evaluated.

The response time of the BGB strain sensor was determined under the condition of applying a step tensile strain of 0.2% with a tensile speed of 40 mm/s. As shown in Figure 2d, the response time is about 120 ms. To measure the detection limit (Figure 2e), a series of gradually ascending step tensile strains (0.01, 0.02, 0.04 and 0.06%) were applied to the BGB strain sensor, which suggests that the detection limit of strain loading can be as minute as 0.01%, exhibiting high potentials for monitoring subtle strain signals in practical applications. Figure 2f presents the hysteresis effect of the BGB strain sensor during the first stretching–releasing cyclic process at the strain of 30%, illustrating that this BGB sensor experiences an irreversibly relative resistance change of 79.46% when released back to the initial state. The hysteresis phenomenon exists in a majority of reported flexible strain sensors,[36,37] and this behavior can be explained by the viscoelastic nature of the dragon skin and the interface interaction between graphene and the dragon skin.[13] Despite this, the hysteresis effect exhibited here is low, confirmed by the high consistency of the two resistance response curves under the first stretching–releasing cyclic process. Besides, as shown in Figure S6, the BGB strain sensor demonstrates a low hysteresis effect at the strain of 10 and 50%, elucidating the high reliability of the BGB strain sensor in wearable devices. To study the overshoot performance of the BGB strain sensor, the BGB strain sensor

was loaded with an instantaneous strain of 30% (stretching speed: 40 mm/s) and subsequently this tension state was kept. As revealed in Figure 2g, after the sudden application of tensile loading, the current can quickly reach the steady state within 4 s, indicating a low overshoot performance, which is comparable with[38] and even superior to[39] other reported strain sensors. The durability of the BGB strain sensor was evaluated by measuring the relative resistance variation under multiple loading cycles. As exhibited in Figure 2h, when the BGB strain sensor experiences the stretching–releasing cycles at the strain of 30%, although there is a slight downshift of the relative resistance variation at the maximum tensile strain during the first 25 cycles, this strain sensor functions relatively stable from 25 to more than 6000 cycles. Whereas the BGB strain sensor experiences the stretching–releasing cycles under the loading of 15% strain (Figure S7), despite showing a little signal degradation during the first 15 cycles, the response curves remain nearly constant from 15 to more than 6000 cycles, demonstrating reliable durability.

3.3. Working Mechanism Analysis of the BGB Strain Sensor. To investigate the sensing mechanism of the BGB strain sensor, the morphology variations of the BGB sensing film under tensile strain from 0 to 60% were traced through SEM characterization. As exhibited in Figure 3a,b, before
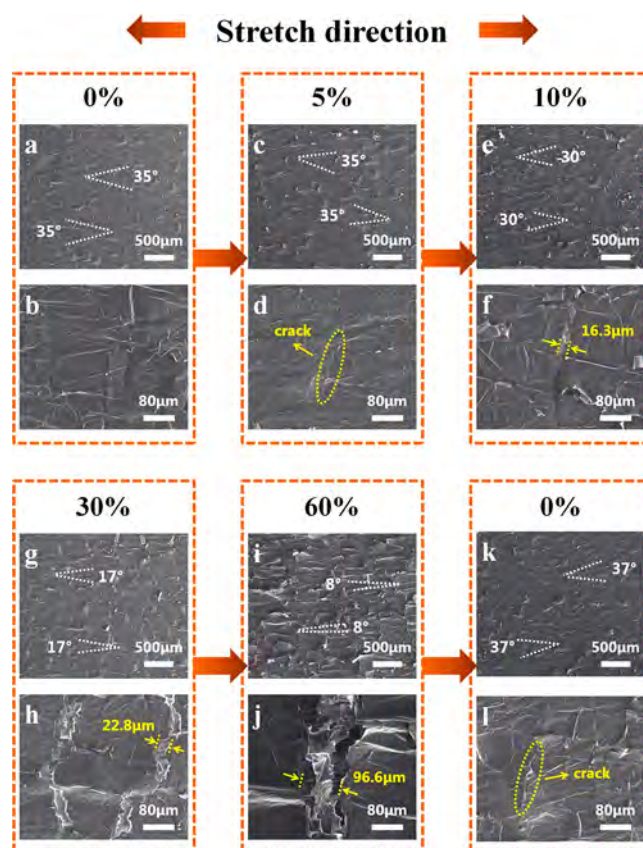

Figure 3. (a,b) Top-view SEM images of the BGB sensing film at 0% strain. (c,d) Top-view SEM images of the BGB sensing film at 5% strain. (e,f) Top-view SEM images of the BGB sensing film at 10% strain. (g,h) Top-view SEM images of the BGB sensing film at 30% strain. (i,j) Top-view SEM images of the BGB sensing film at 60% strain. (k,l) Top-view SEM images of the BGB sensing film released back to 0% strain (the skew angles and cracks-related indicators are marked as white and yellow, respectively.).

tensile stress loading, graphene belts possessing two different orientations braided regularly with the skew angle of 35°, and some wrinkles on the sensing film were observed. Subsequently, as shown in Figure 3c,d, when the tensile strain was increased to 5%, the skew angle of the graphene belts was still 35°; however, wrinkles perpendicular to the stretch direction disappeared and some cracks were initiated. When the BGB strain sensor experienced a tensile strain of 10% (Figure 3e,f), new cracks formed and the originally formed ones propagated to the width of approximately 16.3 μm. Additionally, the braided structure still remained and the skew angle between graphene belts decreased to 30°. Here, the rotation of graphene belts results from the existence of the skew angle. Because of the skew angle, the stretching strain (ε) can be decomposed to $\varepsilon_{//}$ and $\varepsilon_{\perp}$; $\varepsilon_{//}$ is marked as the strain aligned with the belts and $\varepsilon_{\perp}$ means the corresponding strain perpendicular to the belts. $\varepsilon_{\perp}$ makes the belts revolve, whereas $\varepsilon_{//}$ elongates the belts, and the belts will fracture as $\varepsilon_{//}$ exceeds ε_{ut} (Ultimate Tensile Strain). Furthermore, when the BGB strain sensor was stretched to 30% (Figure 3g,h), new cracks formed and the original ones continued to elongate both laterally and longitudinally, with the average width of around 22.8 μm. Besides, the skew angle between graphene belts turned to 17° and the braided structure still remained. Figure 3i,j exhibits the morphology of the strain sensor under 60% tensile strain. Here, the braided morphology still existed, and the skew angle between the graphene belts experienced a decrease to 8°, indicating that the orientation of graphene belts was nearly parallel to the tensile direction. Additionally, cracks enlarged transversely to connect each other and simultaneously broadened longitudinally to the width of 96.6 μm. When the strain was removed, the BGB strain sensor released back to the initial state, as shown in Figure 3k,l. Although the skew angle between oriented graphene belts returned to the initial value of around 37° and the structure of braided belts still remained, the cracks produced during the process of stretching could not completely vanish. Accordingly, the relative resistance variation was unable to come back to 0, explaining the generation of irreversible resistance variation, which is consistent with the results of the hysteresis effect as discussed above.

From the above analysis, we can reasonably speculate that the skew angle and intersection regions of the BGB sensing film are two key factors enabling the BGB strain sensor with both a wide sensing range and high sensitivity within the entire working strain, as schematically illustrated in Figure 4. On one hand, the existence of the skew angle is beneficial to the rotation of graphene belts, which can effectively delocalize strain stress and keep the braided structure, thus enhancing the sensing range of the strain sensor. On the other hand, the
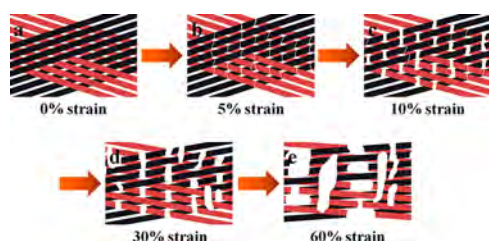
intersection regions of the graphene belts with various orientations can be regarded as the area of concentrating stress. When under tensile loading, the intersection regions promote the rapid formation and subsequently continuous enlargement of cracks, which is responsible for the drastic increase of the resistance, guaranteeing high sensitivity of the BGB strain sensor over the full sensing range. To further prove this mechanism, finite element analysis was conducted. As shown in Tables S2 and S3, when the belts were stretched, the belts rotated, and the braided structure still remained, which was consistent with the SEM analysis as discussed above. Besides, the districts of stress and strain concentration appeared highly close to the intersection area of the belts, promoting the formation and subsequent propagation of cracks, which also agreed with the results as discussed above.

3.4. Demonstration of Full-Range Human Motion Monitoring.

In order to demonstrate the application potentials of the BGB strain sensor as a wearable device for full-range human activities' recognition, as shown in Figure 5d, the BGB strain sensor was attached to the table or different human skin parts of a human body with the assistance of medical tape. On one hand, on account of a large sensing range, the BGB strain sensor has great responsiveness to vigorous joint actions. Figure 5b shows the step curves stemming from finger-bending motions, indicating its application potentials in the field of gesture control. Additionally, various motions associated with the knee such as jogging, jumping, and squatting can be differentiated by virtue of the correspondingly responsive patterns, suggesting its promising potential of sports performance monitoring[40] (Figure 5c). For the other, the BGB strain sensor is also capable of capturing subtle physiological signals because of ultralow detection limit and high sensitivity under small strain stimuli. In Figure 5a, the BGB strain sensor can differentiate diverse words such as "Strain", "Sensor", "Graphene", and "Copper" via the exhibition of distinct signals, as a consequence of a strong response to the movements from the epidermis/muscle around the throat during phonation,[25] showing great potential in the application fields like speech recognition[41] and voice recovery training.[42] As illustrated in Figure 5e, the BGB strain sensor is able to recognize the signals produced from regular blowing, demonstrating favorable capabilities in the domain like noncontact human health monitoring.[43,44] Figure 5f presents the patterns of chest muscle movements generated by breathing, and two consecutive peaks in one periodic profile attributed to the heartbeat are clearly recorded, meaning that this BGB strain sensor can be leveraged in disease diagnosis[45] such as myocarditis, arrhythmia, coronary heart disease, and so forth. Besides, in Figure 5g, the characteristic profile of subtle wrist pulses, with each composed of three peaks orderly named as percussion peaks (P), tidal peaks (T), and diastolic peaks (D) according to a previous report,[46] is distinctly and periodically recorded. Consider that wrist pulse is one of the most significant indicators in human health monitoring, such a result in Figure 5g is again indicative of the BGB strain sensor's promising function in disease diagnosis, such as hyperthyroidism and jaundice. Based on the results exhibited in Figure 5 and the corresponding analysis, our BGB strain sensor possesses great potential in full-range detection of human motions, and even personal healthcare owing to its features of a large sensing range, high sensitivity during the whole strain range, and extremely low detection limit.
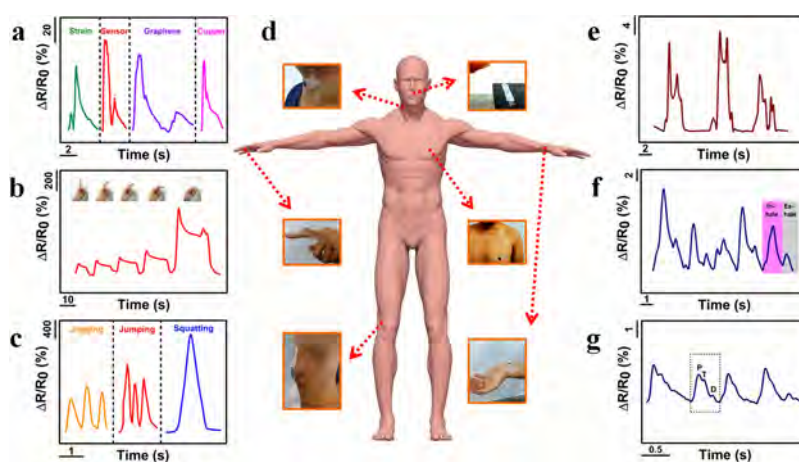

Figure 4. Schematic diagram of the top-view of the BGB conductive film at different strains in the first stretching test (the belts with different orientations are marked as black and pink, respectively, and the cracks among the belts are marked as white).

Figure 5. Wearable applications of the BGB strain sensors for detecting human movements. (a) Responsive signal variations of the wearable sensor attached to the throat when the wearer spoke "Strain", "Sensor", "Graphene", and "Copper", respectively. (b) Responsive signal variations of the wearable sensor on the finger in a multistep bending process (inset images illustrate the finger-bending positions). (c) Responsive signal variations of the wearable sensor sticking to the knee under human actions of jogging, jumping, and squatting, respectively. (d) Schematic illustration of a 3D manikin and photographs showing the wearable sensors adhered on to different parts of the human body or the table. (e) Responsive signal variations of the wearable sensor in a blowing test. (f) Responsive signal variations of the wearable sensor attached to the chest in a breathing process (inhaling part and exhaling part of one periodic profile were marked as pink and gray, respectively). (g) Responsive signal variations of a wearable sensor on the wrist in a process of pulse monitoring (P-peak, T-peak, and D-peak were separately marked in one periodic profile).

4. CONCLUSIONS

In summary, a BGB flexible strain sensor exhibits an excellent integration of a wide sensing range (55.55% strain), high sensitivity (GF > 175.16 over the whole sensing range), ultralow limit of detection (0.01% strain), low hysteresis (10, 30, and 50% tensile strain), and reliable dynamic repeatability (>6000 cycles at 10 and 30% strain). A series of SEM observations reveal that the intersection regions and skew angle of the sensing belts are responsible for the desirable performance. The intersection regions promote the rapid initiation and elongation of cracks under tensile loading, leading to a drastic increase in the resistance and thus guaranteeing high sensitivity over the entire sensing range, whereas the skew angle causes the rotation of the graphene belts, which disperses stress and retains the intactness of the braided morphology, and therefore ensures a wide sensing range. As strain sensors, the practical applications of monitoring human motions from slight stimuli to vigorous activities are demonstrated, suggesting the great potential of the BGB strain sensor in the emerging wearable electronic devices. Furthermore, the excellent architecture and the facile fabrication method can be extended to other sensing materials and relevant flexible electronics.

■ ASSOCIATED CONTENT

ⓢ Supporting Information

The Supporting Information is available free of charge at https://pubs.acs.org/doi/10.1021/acsami.9b21921.

> SEM images of braided Cu belts before and after the growth of graphene; optical image of the BGB strain sensor in the bending state; Raman spectrum of the BGB strain sensing film; optical photograph of the graphene film on the dragon skin (precured time: 0, 1.5, and 3 min); optical images of the conductive layer arranged horizontally and vertically on the flexible substrate; hysteresis results of the BGB strain sensor under the strain of 10 and 50%; durability curves of the BGB strain sensor under the strain of 15%; comparison of sensing properties in previously reported strain sensors; and simulation information and the FEA process of the braided belts during stretching (PDF)

■ AUTHOR INFORMATION

Corresponding Authors

Ranran Wang — State Key Laboratory of High Performance Ceramics and Superfine Microstructure, Shanghai Institute of Ceramics, Chinese Academy of Sciences, Shanghai 200050, P. R. China; Email: wangranran@mail.sic.ac.cn

Jing Sun — State Key Laboratory of High Performance Ceramics and Superfine Microstructure, Shanghai Institute of Ceramics, Chinese Academy of Sciences, Shanghai 200050, P. R. China; orcid.org/0000-0003-1101-1584; Email: jingsun@mail.sic.ac.cn

Authors

Yuxiang Li — State Key Laboratory of High Performance Ceramics and Superfine Microstructure, Shanghai Institute of Ceramics, Chinese Academy of Sciences, Shanghai 200050, P. R. China; Center of Materials Science and Optoelectronics Engineering, University of Chinese Academy of Sciences, Beijing 100049, P. R. China

Tengyu He — State Key Laboratory of High Performance Ceramics and Superfine Microstructure, Shanghai Institute of Ceramics, Chinese Academy of Sciences, Shanghai 200050, P. R. China

Liangjing Shi — State Key Laboratory of High Performance Ceramics and Superfine Microstructure, Shanghai Institute of Ceramics, Chinese Academy of Sciences, Shanghai 200050, P. R. China

Complete contact information is available at:
https://pubs.acs.org/10.1021/acsami.9b21921

Author Contributions

Y.L. and T.H. contributed equally to this work. The paper was written through contributions of all the authors. All the authors have given approval to the final version of the paper.

Notes

The authors declare no competing financial interest.

■ REFERENCES

(1) Qiu, A.; Li, P.; Yang, Z.; Yao, Y.; Lee, I.; Ma, J. A Path Beyond Metal and Silicon:Polymer/Nanomaterial Composites for Stretchable Strain Sensors. *Adv. Funct. Mater.* **2019**, 29, 1806306.

(2) Zhu, M.; Inomata, N.; Adachi, N.; Sakurai, A.; Nomura, M.; Ono, T. High-Gauge Factor Strain Sensor Based on Piezoelectric Aluminum Nitride Coupled to MOSFET. *IEEE Sens. J.* **2019**, 19, 3626−3632.

(3) Wang, Y.; Gong, S.; Wang, S. J.; Yang, X.; Ling, Y.; Yap, L. W.; Dong, D.; Simon, G. P.; Cheng, W. Standing Enokitake-like Nanowire Films for Highly Stretchable Elastronics. *ACS Nano* **2018**, 12, 9742−9749.

(4) Zhu, B.; Gong, S.; Cheng, W. Softening Gold for Elastronics. *Chem. Soc. Rev.* **2019**, 48, 1668−1711.

(5) Bai, W.; Kuang, T.; Chitrakar, C.; Yang, R.; Li, S.; Zhu, D.; Chang, L. Patchable Micro/Nanodevices Interacting with Skin. *Biosens. Bioelectron.* **2018**, 122, 189−204.

(6) Gong, S.; Yap, L. W.; Zhu, B.; Zhai, Q.; Liu, Y.; Lyu, Q.; Wang, K.; Yang, M.; Ling, Y.; Lai, D. T. H.; Marzbanrad, W. Local Crack-Programmed Gold Nanowire Electronic Skin Tattoos for In-Plane Multisensor Integration. *Adv. Mater.* **2019**, 31, 1903789.

(7) Zhang, J.; Cao, Y.; Qiao, M.; Ai, L.; Sun, K.; Mi, Q.; Zang, S.; Zuo, Y.; Yuan, X.; Wang, Q. Human Motion Monitoring in Sports Using Wearable Graphene-Coated Fiber Sensors. *Sens. Actuators, A* **2018**, 274, 132−140.

(8) Yang, J.; Liu, Q.; Deng, Z.; Gong, M.; Lei, F.; Zhang, J.; Zhang, X.; Wang, Q.; Liu, Y.; Wu, Z.; Guo, C. F. Ionic liquid-activated wearable electronics. *Mater. Today Phys.* **2019**, 8, 78−85.

(9) Zhang, Y.; Hu, Y.; Zhu, P.; Han, F.; Zhu, Y.; Sun, R.; Wong, C.-P. Flexible and Highly Sensitive Pressure Sensor Based on Microdome-Patterned PDMS Forming with Assistance of Colloid Self-Assembly and Replica Technique for Wearable Electronics. *ACS Appl. Mater. Interfaces* **2017**, 9, 35968−35976.

(10) Webb, R. C.; Bonifas, A. P.; Behnaz, A.; Zhang, Y.; Yu, K. J.; Cheng, H.; Shi, M.; Bian, Z.; Liu, Z.; Kim, Y.-S.; Yeo, W.-H.; Park, J. S.; Song, J.; Li, Y.; Huang, Y.; Gorbach, A. M.; Rogers, J. A. Ultrathin Conformal Devices for Precise and Continuous Thermal Characterization of Human Skin. *Nat. Mater.* **2013**, 12, 938−944.

(11) Liao, X.; Zhang, Z.; Kang, Z.; Gao, F.; Liao, Q.; Zhang, Y. Ultrasensitive and Stretchable Resistive Strain Sensors Designed for Wearable Electronics. *Mater. Horiz.* **2017**, 4, 502−510.

(12) Wang, Y.; Wang, Y.; Yang, Y. Graphene-Polymer Nanocomposite-Based Redox-Induced Electricity for Flexible Self-Powered Strain Sensors. *Adv. Energy Mater.* **2018**, 8, 1800961.

(13) Amjadi, M.; Kyung, K.-U.; Park, I.; Sitti, M. Stretchable, Skin-Mountable, and Wearable Strain Sensors and Their Potential Applications: A Review. *Adv. Funct. Mater.* **2016**, 26, 1678−1698.

(14) Shi, X.; Liu, S.; Sun, Y.; Liang, J.; Chen, Y. Lowering Internal Friction of 0D-1D-2D Ternary Nanocomposite-Based Strain Sensor by Fullerene to Boost the Sensing Performance. *Adv. Funct. Mater.* **2018**, 28, 1800850.

(15) Pan, F.; Chen, S.-M.; Li, Y.; Tao, Z.; Ye, J.; Ni, K.; Yu, H.; Xiang, B.; Ren, Y.; Qin, F.; Yu, S.-H.; Zhu, Y. 3D Graphene Films Enable Simultaneously High Sensitivity and Large Stretchability for Strain Sensors. *Adv. Funct. Mater.* **2018**, 28, 1803221.

(16) Zheng, Y.; Jin, Q.; Chen, W.; Sun, Y.; Wang, Z. High Sensitivity and Wide Sensing Range of Stretchable Sensors with Conductive Microsphere Array Structures. *J. Mater. Chem. C* **2019**, 7, 8423−8431.

(17) Drotlef, D.-M.; Amjadi, M.; Yunusa, M.; Sitti, M. Bioinspired Composite Microfibers for Skin Adhesion and Signal Amplification of Wearable Sensors. *Adv. Mater.* **2017**, 29, 1701353.

(18) Kang, D.; Pikhitsa, P. V.; Choi, Y. W.; Lee, C.; Shin, S. S.; Piao, L.; Park, B.; Suh, K.-Y.; Kim, T.-i.; Choi, M. Ultrasensitive Mechanical Crack-Based Sensor Inspired by the Spider Sensory System. *Nature* **2014**, 516, 222−226.

(19) Wang, Y.; Wang, L.; Yang, T.; Li, X.; Zang, X.; Zhu, M.; Wang, K.; Wu, D.; Zhu, H. Wearable and Highly Sensitive Graphene Strain Sensors for Human Motion Monitoring. *Adv. Funct. Mater.* **2014**, 24, 4666−4670.

(20) Xue, Z.; Song, H.; Rogers, J. A.; Zhang, Y.; Huang, Y. Mechanically-Guided Structural Designs in Stretchable Inorganic Electronics. *Adv. Mater.* **2019**, 1902254.

(21) Liu, Z.; Wang, H.; Huang, P.; Huang, J.; Zhang, Y.; Wang, Y.; Yu, M.; Chen, S.; Qi, D.; Wang, T.; Jiang, Y.; Chen, G.; Hu, G.; Li, W.; Yu, J.; Luo, Y.; Loh, X. J.; Liedberg, B.; Li, G.; Chen, X. Highly Stable and Stretchable Conductive Films through-Thermal-Radiation-Assisted Metal Encapsulation. *Adv. Mater.* **2019**, 31, 1901360.

(22) He, T.; Lin, C.; Shi, L.; Wang, R.; Sun, J. Through-Layer Buckle Wavelength-Gradient Design for the Coupling of High Sensitivity and Stretchability in a Single Strain Sensor. *ACS Appl. Mater. Interfaces* **2018**, 10, 9653−9662.

(23) Tsen, A. W.; Brown, L.; Havener, R. W.; Park, J. Polycrystallinity and Stacking in CVD Graphene. *Acc. Chem. Res.* **2013**, 46, 2286−2296.

(24) Martins Ferreira, E. H.; Moutinho, M. V. O.; Stavale, F.; Lucchese, M. M.; Capaz, R. B.; Achete, C. A.; Jorio, A. Evolution of the Raman Spectra from Single-, Few-, and Many-Layer Graphene with Increasing Disorder. *Phys. Rev. B: Condens. Matter Mater. Phys.* **2010**, 82, 125429.

(25) Zhao, J.; Wang, G.; Yang, R.; Lu, X.; Cheng, M.; He, C.; Xie, G.; Meng, J.; Shi, D.; Zhang, G. Tunable Piezoresistivity of Nanographene Films for Strain Sensing. *ACS Nano* **2015**, 9, 1622−1629.

(26) Liu, Q.; Chen, J.; Li, Y.; Shi, G. High-Performance Strain Sensors with Fish-Scale-Like Graphene-Sensing Layers for Full-Range Detection of Human Motions. *ACS Nano* **2016**, 10, 7901−7906.

(27) Ling, S.; Wang, Q.; Zhang, D.; Zhang, Y.; Mu, X.; Kaplan, D. L.; Buehler, M. J. Integration of Stiff Graphene and Tough Silk for the Design and Fabrication of Versatile Electronic Materials. *Adv. Funct. Mater.* **2018**, 28, 1705291.

(28) Cai, Y.; Shen, J.; Ge, G.; Zhang, Y.; Jin, W.; Huang, W.; Shao, J.; Yang, J.; Dong, X. Stretchable Ti3C2Tx MXene/Carbon Nanotube Composite Based Strain Sensor with Ultrahigh Sensitivity and Tunable Sensing Range. *ACS Nano* **2018**, 12, 56−62.

(29) Hwang, B.-U.; Lee, J.-H.; Trung, T. Q.; Roh, E.; Kim, D.-I.; Kim, S.-W.; Lee, N.-E. Transparent Stretchable Self-Powered Patchable Sensor Platform with Ultrasensitive Recognition of Human Activities. *ACS Nano* **2015**, 9, 8801−8810.

(30) Yan, C.; Wang, J.; Kang, W.; Cui, M.; Wang, X.; Foo, C. Y.; Chee, K. J.; Lee, P. S. Highly Stretchable Piezoresistive Graphene-Nanocellulose Nanopaper for Strain Sensors. *Adv. Mater.* **2014**, 26, 2022−2027.

(31) Zeng, Z.; Yu, Y.; Song, Y.; Tang, N.; Ye, L.; Zang, J. Precise Engineering of Conductive Pathway by Frictional Direct-Writing for Ultrasensitive Flexible Strain Sensors. *ACS Appl. Mater. Interfaces* **2017**, 9, 41078−41086.

(32) Liao, X.; Liao, Q.; Yan, X.; Liang, Q.; Si, H.; Li, M.; Wu, H.; Cao, S.; Zhang, Y. Flexible and Highly Sensitive Strain Sensors Fabricated by Pencil Drawn for Wearable Monitor. *Adv. Funct. Mater.* **2015**, 25, 2395−2401.

(33) Lee, T.; Choi, Y. W.; Lee, G.; Pikhitsa, P. V.; Kang, D.; Kim, S. M.; Choi, M. Transparent ITO Mechanical Crack-based Pressure and Strain Sensor. *J. Mater. Chem. C* **2016**, *4*, 9947−9953.

(34) Zhang, W.; Zhu, R.; Nguyen, V.; Yang, R. Highly Sensitive and Flexible Strain Sensors based on Vertical Zinc Oxide Nanowire Arrays. *Sens. Actuators, A* **2014**, *205*, 164−169.

(35) Ho, M. D.; Ling, Y.; Yap, L. W.; Wang, Y.; Dong, D.; Zhao, Y.; Cheng, W. Percolating Network of Ultrathin Gold Nanowires and Silver Nanowires toward "Invisible" Wearable Sensors for Detecting Emotional Expression and Apexcardiogram. *Adv. Funct. Mater.* **2017**, *27*, 1700845.

(36) Deng, H.; Ji, M.; Yan, D.; Fu, S.; Duan, L.; Zhang, M.; Fu, Q. Towards Tunable Resistivity-Strain Behavior through Construction of Oriented and Selectively Distributed Conductive Networks in Conductive Polymer Composites. *J. Mater. Chem. A* **2014**, *2*, 10048−10058.

(37) Amjadi, M.; Pichitpajongkit, A.; Lee, S.; Ryu, S.; Park, I. Highly Stretchable and Sensitive Strain Sensor based on Silver Nanowire−Elastomer Nanocomposite. *ACS Nano* **2014**, *8*, 5154−5163.

(38) Cheng, Y.; Wang, R.; Sun, J.; Gao, L. A Stretchable and Highly Sensitive Graphene-based Fiber for Sensing Tensile Strain, Bending, and Torsion. *Adv. Mater.* **2015**, *27*, 7365−7371.

(39) Mattmann, C.; Clemens, F.; Tröster, G. Sensor for Measuring Strain in Textile. *Sensors* **2008**, *8*, 3719−3732.

(40) Boland, C. S.; Khan, U.; Backes, C.; O'Neill, A.; McCauley, J.; Duane, S.; Shanker, R.; Liu, Y.; Jurewicz, I.; Dalton, A. B. Sensitive, High-Strain, High-Rate Bodily Motion Sensors Based on Graphene-Rubber Composites. *ACS Nano* **2014**, *8*, 8819−8830.

(41) Shimada, K.; Bando, Y.; Mimura, M.; Itoyama, K.; Yoshii, K.; Kawahara, T. Unsupervised Speech Enhancement Based on Multi-channel NMF-Informed Beamforming for Noise-Robust Automatic Speech Recognition. *IEEE-ACM Trans. Audio Speech Lang.* **2019**, *27*, 960−971.

(42) Lin, L.; Sun, N.; Yang, Q.; Zhang, Y.; Shen, J.; Shi, L.; Fang, Q.; Sun, G. Effect of Voice Training in the Voice Rehabilitation of Patients with Vocal Cord Polyps after Surgery. *Exp. Ther. Med.* **2014**, *7*, 877−880.

(43) Shahshahani, A.; Laverdiere, C.; Bhadra, S.; Zilic, Z. Ultrasound Sensors for Diaphragm Motion Tracking: An Application in Non-Invasive Respiratory Monitoring. *Sensors* **2018**, *18*, 2617.

(44) Wang, T.; Zhang, Y.; Liu, Q.; Cheng, W.; Wang, X.; Pan, L.; Xu, B.; Xu, H. A Self-Healable, Highly Stretchable, and Solution Processable Conductive Polymer Composite for Ultrasensitive Strain and Pressure Sensing. *Adv. Funct. Mater.* **2018**, *28*, 1705551.

(45) Pang, C.; Lee, G.-Y.; Kim, T.-i.; Kim, S. M.; Kim, H. N.; Ahn, S.-H.; Suh, K.-Y. A Flexible and Highly Sensitive Strain-Gauge Sensor Using Reversible Interlocking of Nanofibres. *Nat. Mater.* **2012**, *11*, 795−801.

(46) Wang, X.; Gu, Y.; Xiong, Z.; Cui, Z.; Zhang, T. Silk-Molded Flexible, Ultrasensitive, and Highly Stable Electronic Skin for Monitoring Human Physiological Signals. *Adv. Mater.* **2014**, *26*, 1336−1342.